6th European Conference on Computational Mechanics (ECCM 6)
7th European Conference on Computational Fluid Dynamics (ECFD 7)
11–15 June 2018, Glasgow, UK

ADAPTIVE SAMPLING CRITERIA FOR MULTI-FIDELITY METAMODELS IN CFD-BASED SHAPE OPTIMIZATION

RICCARDO PELLEGRINI[1], ANDREA SERANI[1], MATTEO DIEZ[1], JEROEN WACKERS[2], PATRICK QUEUTEY[2], AND MICHEL VISONNEAU[2]

[1] CNR-INM, National Research Council-Institute of Marine Engineering
Via di Vallerano 139, 00128 Rome, Italy
{riccardo.pellegrini; andrea.serani}@insean.cnr.it; matteo.diez@cnr.it

[2] LHEEA Lab, Ecole Centrale de Nantes, CNRS-UMR 6598, 44321 Nantes Cedex 3, France
{jeroen.wackers; patrick.queutey; michel.visonneau}@ec-nantes.fr

Key words: Shape Optimization, Adaptive Grid Refinement, Adaptive Sampling, Multi-Fidelity Metamodels, RANS

Abstract. The paper presents a study on four adaptive sampling methods of a multi-fidelity global metamodel for expensive computer simulations. The multi-fidelity approximation is built as the sum of a low-fidelity-trained metamodel and the metamodel of the difference between high- and low-fidelity simulations. The multi-fidelity metamodel is trained selecting the fidelity to sample based on the prediction uncertainty and the computational cost ratio between the high- and low-fidelity evaluations. The adaptive sampling methods are applied to the CFD-shape optimization of a NACA hydrofoil. The performance of the sampling methods is assessed in terms of convergence of the maximum uncertainty and the minimum of the function.

1 INTRODUCTION

Fluid-dynamic shape design of aerial, ground, and water-borne vehicles demand the use of high-fidelity numerical solvers with large computational grids to assess accurately the design performance and make sound design decisions. The latter can be achieved by combining the computational fluid dynamics (CFD) analysis with a shape/design modification tool (CAD) and a minimization algorithm into an automatic simulation-based design optimization (SBDO). High-fidelity physics-based solvers results in computationally expensive analyses. Furthermore, the optimization algorithm may require a large number of function evaluations to converge to the final solution. Therefore, the resulting computational cost could become very high, making SBDO unaffordable for most users and projects for which limited computational resources and time are usually available.

In order to reduce the computational cost of the SBDO process, metamodeling methods have been developed and successfully applied in several engineering fields [1]. Metamodel

performance depends on several concurrent issues, such as the dimensionality of the problem, the nature (smooth or noisy) of the function, and the sampling approach [2] used for its training. A priori sampling provides distribution of training-set points, without any knowledge of the function. Sequential sampling adds new training points iteratively, based on the knowledge gathered during the training process. An adaptive sampling for dynamic stochastic radial basis functions (SRBF) has been presented in [3] and compared to dynamic Kriging [4]. A multi-criteria adaptive sampling method for dynamic SRBF has been presented in [5] for design optimization problems.

In addition to metamodels, multi-fidelity (or variable-fidelity) approximation methods have been developed with the aim of combining to some extent the accuracy of high-fidelity solvers with the computational cost of low-fidelity solvers. Combining metamodeling methods with multi-fidelity approximations potentially leads to a further reduction of the computational cost of the SBDO procedure. Additive and/or multiplicative correction methods might be used to build multi-fidelity metamodels, using high- and low-fidelity evaluations [6, 7, 9]. Several metamodels can be used with multi-fidelity data, as co-kriging [8] and RBF [10].

The objective of the present work is the assessment of four adaptive sampling methods for multi-fidelity metamodeling. These are based on the maximum prediction uncertainty, a multi-fidelity version of the expected improvement [11], the maximum prediction uncertainty and the objective function through an aggregated merit factor, and the multi-criteria based on the maximum prediction uncertainty and the objective function [5]. These methods are applied to the CFD-based shape optimization of a NACA hydrofoil, addressing the drag minimization at Re $= 8.41E6$. The hydrofoil hydrodynamic performance is assessed by RANSE solver ISIS-CFD, developed at Ecole Centrale de Nantes/CNRS and integrated in the FINE/Marine simulation suite from NUMECA Int. Mesh deformation techniques and adaptive grid refinement techniques are adopted to allow the automatic shape deformation of the hydrofoil. The high- and low-fidelity are defined by the grid refinement. The performance of the adaptive sampling methods are assessed in terms of prediction uncertainty and optimization procedure convergence.

2 MULTI-FIDELITY METAMODELING

Consider an objective function $f(\mathbf{x})$, where $\mathbf{x} \in \mathbb{R}^N$ is the design variable vector and N the design space dimension. The multi-fidelity prediction $\hat{f}(\mathbf{x})$ is defined by an additive correction to a low-fidelity trained metamodel $\widetilde{f}_L(\mathbf{x})$ as

$$\hat{f}(\mathbf{x}) = \tilde{f}_L(\mathbf{x}) + \tilde{\varepsilon}(\mathbf{x}) \tag{1}$$

where the correction is provided by the metamodel of the error $\tilde{\varepsilon}(\mathbf{x})$, defined by the difference between high- (HF) and low-fidelity (LF) evaluations (f_H and f_L) [9] as

$$\varepsilon(\mathbf{x}) = f_H(\mathbf{x}) - f_L(\mathbf{x}) \tag{2}$$

The training set for $\tilde{f}_L$ is denoted by $\mathcal{L}$, whereas the training set for $\tilde{\varepsilon}$ is denoted by $\mathcal{E} \subseteq \mathcal{L}$. "$\sim$" indicates metamodel prediction and "$\wedge$" indicates multi-fidelity approximation. Using a metamodel that gives both function prediction and its uncertainty and

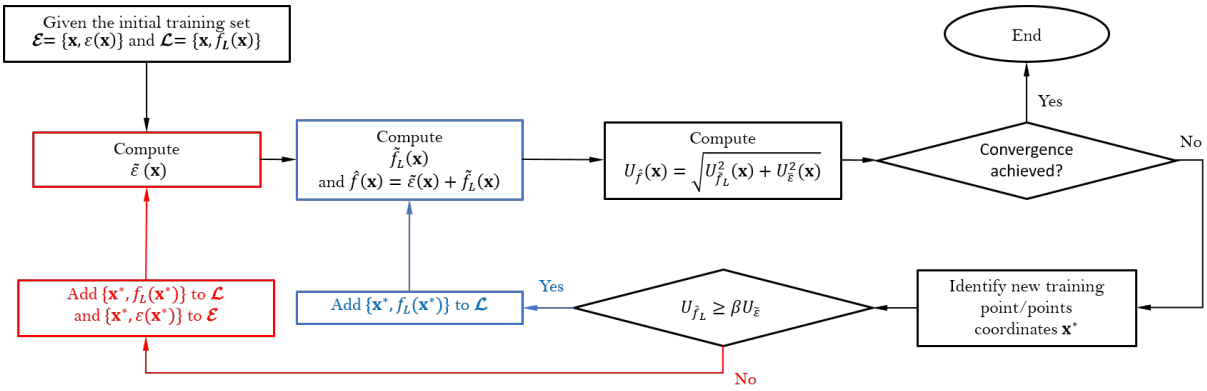

Figure 1: Adaptive multi-fidelity metamodel updating scheme

assuming the uncertainty associate to the low-fidelity and error metamodels ($U_{\tilde{f}_L}$ and $U_{\tilde{\varepsilon}}$ respectively) as uncorrelated, the uncertainty associated to the multi-fidelity prediction can be defined as

$$U_{\hat{f}}(\mathbf{x}) = \sqrt{U^2_{\tilde{f}_L}(\mathbf{x}) + U^2_{\tilde{\varepsilon}}(\mathbf{x})} \tag{3}$$

2.1 Stochastic radial basis functions

The metamodel prediction $\tilde{f}(\mathbf{x})$ is computed as the expected value (EV) over a stochastic tuning parameter of the metamodel $\tau \sim \text{unif}[1,3]$

$$\widetilde{f}(\mathbf{x}) = \text{EV}\left[g(\mathbf{x},\tau)\right]_\tau, \quad \text{with} \quad g(\mathbf{x},\tau) = \sum_{j=1}^{J} w_j ||\mathbf{x}-\mathbf{x}_j||^\tau \tag{4}$$

where w_j are unknown coefficients, $||\cdot||$ is the Euclidean norm, $\mathbf{x}_j$ are the training points with associated objective function value $f(\mathbf{x}_j)$, and J is the number of training points. The coefficients w_j are determined enforcing the interpolation $g(\mathbf{x}_j,\tau) = f(\mathbf{x}_j)$ by solving $\mathbf{A}\mathbf{w} = \mathbf{f}$, with $\mathbf{w} = \{w_j\}$, $a_{i,j} = ||\mathbf{x}-\mathbf{x}_j||^\tau$ and $\mathbf{f} = \{f(\mathbf{x}_j)\}$.

The uncertainty $U_{\widetilde{f}}(\mathbf{x})$ associated with the metamodel prediction is quantified by the 95%-confidence interval of $g(\mathbf{x},\tau)$, evaluated using a Monte Carlo sampling over τ [3].

2.2 Adaptive sampling methods

New training points $\mathbf{x}^\star$ for $\mathcal{L}$ and $\mathcal{E}$ are sequentially defined by the adaptive sampling method, as shown in Fig. 1 and described in the following subsections. Once $\mathbf{x}^\star$ is identified, the training sets $\mathcal{L}$ and $\mathcal{E}$ are updated as

$$\begin{cases} \text{If } U_{\tilde{f}_L}(\mathbf{x}^\star) \geq \beta U_{\tilde{\varepsilon}}(\mathbf{x}^\star), & \text{add } \{\mathbf{x}^\star, f_L(\mathbf{x}^\star)\} \text{ to } \mathcal{L} \\ \text{else,} & \text{add } \{\mathbf{x}^\star, f_L(\mathbf{x}^\star)\} \text{ to } \mathcal{L} \text{ and } \{\mathbf{x}^\star, \varepsilon(\mathbf{x}^\star)\} \text{ to } \mathcal{E} \end{cases} \tag{5}$$

where $\beta \in [0,1]$ is the ratio between the LF and HF computational cost. In the first case, only a low-fidelity evaluation is performed, while the second case requires both low- and high-fidelity evaluations for the same $\mathbf{x}^\star$.

2.2.1 Maximum uncertainty

The maximum uncertainty adaptive sampling (MUAS) has been presented in [9]. This method identifies a new training point by solving the following single-objective maximization problem

$$\mathbf{x}^\star = \underset{\mathbf{x}}{\text{argmax}}[U_{\hat{f}}(\mathbf{x})] \tag{6}$$

2.2.2 Multi-fidelity expected improvement

Since the multi-fidelity concept is to keep the high-fidelity training set as small as possible, the expected improvement proposed in [11] is extended here to a multi-fidelity expected improvement (MFEI) as

$$\text{MFEI}\left(\mathbf{x}\right) = \text{EV}\left[\max\left(f_{\min} - g\left(\mathbf{x},\tau\right),0\right)\right]_\tau, \quad \text{with} \quad f_{\min} = \min\left[\hat{f}(\mathbf{x})\right] \tag{7}$$

where $g\left(\mathbf{x},\tau\right)$ is a stochastic multi-fidelity prediction. The MFEI is therefore the expected value of potential reduction provided by all the SRBF with respect to the predicted minimum, at the present iteration of the sampling process.

The MFEI adaptive sampling identifies a new training point by solving the following single-objective maximization problem

$$\mathbf{x}^\star = \underset{\mathbf{x}}{\text{argmax}}[\text{MFEI}(\mathbf{x})] \tag{8}$$

2.2.3 Aggregate criteria

The aggregate criteria adaptive sampling (ACAS) is based on the difference between the multi-fidelity prediction and the associated uncertainty. ACAS identifies a new training point by solving the following single-objective minimization

$$\mathbf{x}^\star = \underset{\mathbf{x}}{\text{argmin}}[\hat{f}(\mathbf{x}) - U_{\hat{f}}(\mathbf{x})] \tag{9}$$

2.2.4 Multi-criteria

The multi-criteria adaptive sampling (MCAS) [5] identifies N_P new training points (user defined) conditional to both multi-fidelity prediction and the associated uncertainty. A multi-objective optimization problem addressing the minimization of the objective function and the maximization of the prediction uncertainty is solved

$$\begin{aligned} &\text{minimize} && \mathbf{f}(\mathbf{x}) = \{\hat{f}(\mathbf{x}), -U_{\hat{f}}(\mathbf{x})\}^\mathsf{T} \\ &\text{subject to} && U_{\hat{f}}(\mathbf{x}) > U^\star_{\hat{f}} \end{aligned} \tag{10}$$

where $U^\star_{\hat{f}}$ is a user defined parameter used to avoid overfitting in the neighborhood of the minimum [5]. New training points are identified down-sampling the non-dominated solution set produced by Eq. 10. Herein, $U^\star_{\hat{f}} = 0.1\%R$, where R is the function range of the initial high-fidelity training set.

2.3 Single- and multi-objective optimization algorithms

A deterministic single-objective formulation of the particle swarm optimization (DPSO) algorithm [12], is used for the solution of the minimization/maximization problems of Eqs. 6, 8, and 9. Furthermore, it is used for the metamodel-based optimization. A multi-objective extension of DPSO (MODPSO) [13] is used for the solution of Eq. 10.

3 NACA HYDROFOIL TEST PROBLEM

The following minimization problem is solved

$$\begin{array}{rl} \text{minimize} & C_d(\mathbf{x}) \\ \text{subject to} & C_l(\mathbf{x}) = 0.6 \\ \text{and to} & \mathbf{l} \leq \mathbf{x} \leq \mathbf{u} \end{array} \tag{11}$$

where C_d and C_l are respectively the drag and lift coefficient of NACA hydrofoil. $\mathbf{l}$ and $\mathbf{u}$ are the lower and upper bound, respectively, of the design variable vector. The equality constraint on the lift coefficient is necessary to compare different geometries of a lifting hydrofoil. The hydrofoil shape is defined by the general equation for 4-digit NACA foils. In this work, the design variables vector is defined as $\mathbf{x} = \{t, m\}$, with t the thickness and m the camber of the hydrofoil. The thickness ranges between $t \in [0.03, 0.12]$, the camber ranges between $m \in [0.025, 0.07]$, and the location of the maximum camber is set equal to 0.4. The simulations conditions are: velocity $V = 10$ m/s, chord $c = 1$ m, fluid density $\rho = 1026$ kg/m^3, and Reynolds number Re $= 8.41E6$. The CFD simulations are performed with the unstructured two-fluid finite-volume Navier-Stokes solver ISIS-CFD developed at Ecole Centrale de Nantes/CNRS and integrated in the FINE/Marine simulation suite from NUMECA Int.

Two evaluation metrics are used is order to evaluate the effectiveness and the efficiency of the multi-fidelity adaptive sampling methods: (1) the maximum value of the multi-fidelity metamodel uncertainty and (2) the objective function value (high-fidelity evaluated).

The following subsections present details about the CFD analysis

3.1 Mesh deformation

The unstructured hexahedral meshes for the simulations are generated using HEXPRESS. Like for most unstructured mesh generators, the grids created by this mesher may be quite different for geometries that are nearly identical. This could result in numerical noise in the simulations results. Therefore, the simulations of all the candidate geometries are performed on the same mesh, which is deformed to fit each geometry. The deformation algorithm is based on [15]. The mesh is divided in layers of cells around the geometry. Then the displacement from the original to the deformed geometry is computed for the faces on the body and this displacement is propagated through the layers of cells. Two smoothing mechanisms are applied: (i) the displacements are diffused over the faces of a single layer, so the mesh deformation becomes more uniform; (ii) a weighting

technique is applied based on the distance to the body, such that the deformation goes to zero on the outer boundaries.

3.2 Adaptive grid refinement

After the initial mesh deformation to fit each geometry, the final meshes are obtained with adaptive grid refinement [16]. The decision on where to refine the mesh is based on metric tensors [17]. The 3×3 criterion tensors $\mathcal{C}_i$ in each i-th cell are computed from the flow solution, indicating the target size of the cells. In a hexahedral cell, let the cell sizes $\mathbf{d}_{i,j}$ $(j = 1, 2, 3)$ be the vectors between the opposing face centers in the three cell directions. The goal of the grid refinement is to obtain

$$||\mathcal{C}_i \mathbf{d}_{i,j}|| = T_r \quad \forall i, j \tag{12}$$

where T_r is a constant. This is accomplished by refining i-th cells in the j-th direction, until $||\mathcal{C}_i \mathbf{d}_{i,j}||$ no longer exceeds the constant T_r. The refinement criteria are based on the second spatial derivatives of the pressure and velocity.

The interest of this procedure for multi-fidelity optimization is that the cell size in the entire mesh varies proportionally to the threshold T_r [16]. Thus, the precision of the simulation can be adjusted by varying this parameter, which makes it easy to automate multi-fidelity simulations. A further advantage is that this technique allows to perform the mesh deformation on the coarse initial grid, instead of a fine grid where small errors in the placement of the nodes can lead to inverted cells. A potential disadvantage is that the refined grids for the different geometries are not the same, which could introduce noise in the results.

3.3 Dynamic positioning

To maintain a constant lift coefficient the angle of incidence for the hydrofoil is adjusted dynamically during the simulations. At regular intervals, the difference between the target and the actual lift is evaluated. Divided by the theoretical lift slope of 2D foils ($\Delta C_l = 2\pi\Delta\alpha$), this gives a change in angle of attack $\Delta\alpha$, which is applied over a few time steps. Then, the flow is allowed to settle and another $\Delta\alpha$ is computed. The mesh is deformed with an analytical weighting technique, to accommodate the rotation.

4 NUMERICAL RESULTS

The initial training set for the problem is a set of $2N + 1$ points including the domain centre and min/max coordinates for each variable. The initial mesh for both high- and low-fidelity has 2,654 cells, the refinement threshold value T_r is set equal to 0.1 and 0.4 for high- and low-fidelity, respectively. Therefore, the resulting refined fine and coarse meshes have 11k and 3.6k cells, respectively (see Fig. 2a and b). Each HF and LF simulation requires about 13 and 5 minutes of wall-clock time to converge, respectively. The resulting computational cost ratio is $\beta = 0.3$. A budget of 150 simulations is provided for the adaptive sampling methods, considering both HF and LF simulations. The multi-fidelity metamodel-based optimization is performed on a normalized domain $\mathbf{x} \in [0, 1]$.

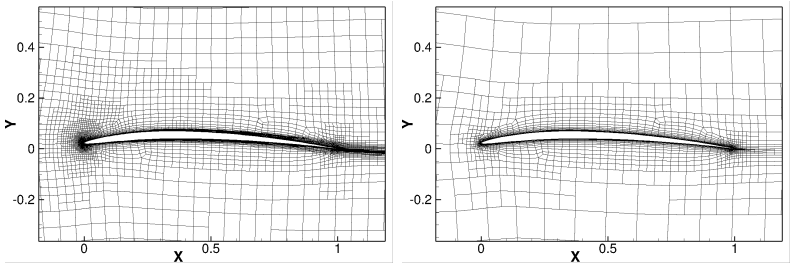

(a) Fine grid, 11k cells (b) Coarse grid, 3.6k cells

Figure 2: Refined computational grids for hydrodynamic simulations

The metamodel-based optimization results are compared to an optimal reference solution for the drag coefficient ($C^{\star}_{d,\min}$) identified by an earlier high-fidelity metamodel-based optimization [18] trained by 150 high-fidelity simulations.

Figure 3 shows the convergences of the maximum prediction uncertainty, the drag coefficient minimum, and the corresponding design variables. MUAS and MCAS achieve lower values of the maximum prediction uncertainty than MFEI and ACAS. On the contrary, only MFEI and ACAS reach a minimum close to the reference. Overall, MFEI provides the fastest convergence towards the minimum. Figure 4 shows the multi-fidelity metamodel prediction and the corresponding training set at final iteration of the four sampling methods. The MUAS and MCAS methods provide a global exploration of the domain. Differently, MFEI and ACAS methods cluster training points in a small region. All the sampling methods use a similar number of HF evaluations (see Tab. 1), with MUAS and MCAS spreading the HF evaluations over the whole domain. Furthermore, it is worth noting that both MUAS and MCAS request HF training points in the domain corners. Differently, MFEI and ACAS methods focus HF evaluations only in the minimum region.

Looking at Fig. 3 it can be noticed how the convergence of the uncertainty prediction of MUAS and MCAS is noisy. This happen since MUAS and MCAS aim at the minimization of the maximum uncertainty, therefore clustering the training points in regions where the uncertainty is high (see Fig. 4). The metamodel uncertainty is affected by a small-scale noise found in the numerical simulations, in regions with clustered training points.

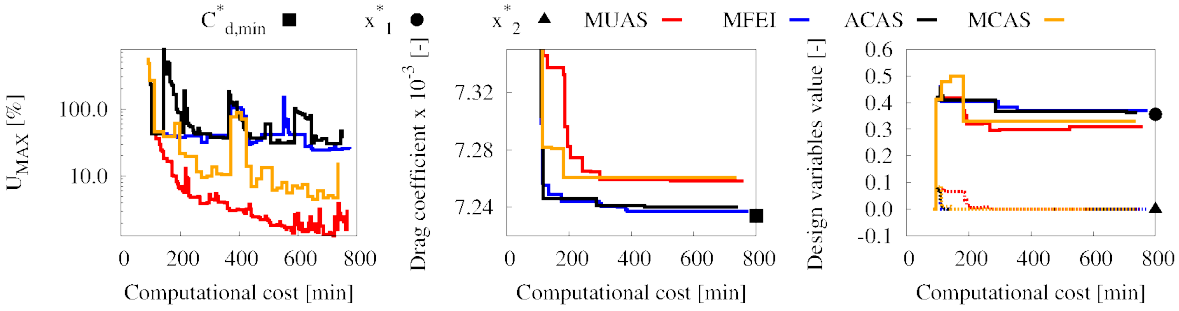

Figure 3: Hydrofoil optimization problem, convergences of the maximum uncertainty, the function minimum, and the function minimum coordinates x_1^* (solid lines) and x_2^* (dashed lines)

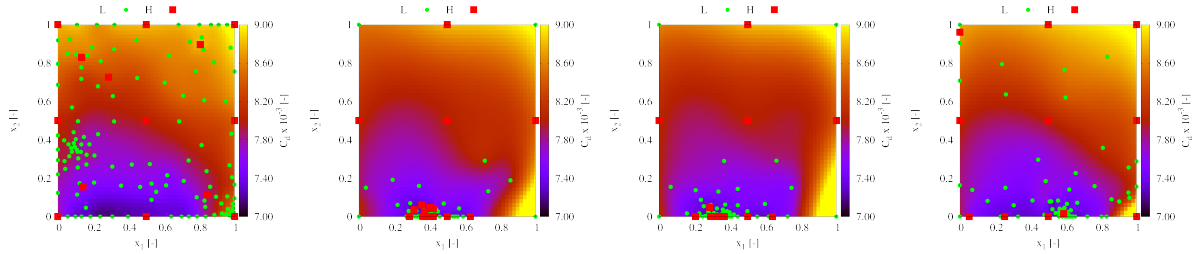

(a) MUAS (b) MFEI (c) ACAS (d) MCAS

Figure 4: Training sets and multi-fidelity metamodel prediction of $C_d(\mathbf{x})$ at the final iteration of the adaptive sampling procedures

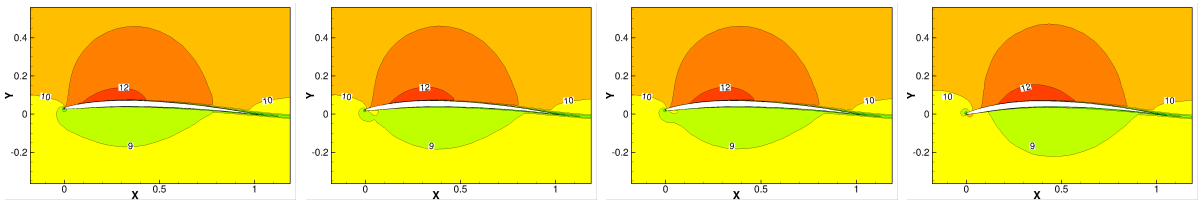

(a) MUAS (b) MFEI (c) ACAS (d) MCAS

Figure 5: Hydrofoil optimization, velocity contour for the optimal configuration identified with the sampling methods

Therefore, MUAS and MCAS add training points in regions where the uncertainty is due to the numerical noise and not to the objective function shape. The effects of the numerical noise are evident in Figs. 4a and 4d. MUAS sampling method clusters samples in the neighborhood of $\mathbf{x} = \{0.1, 0.35\}$ (Fig. 4a), whereas MCAS method clusters samples in the neighborhood of $\mathbf{x} = \{0.6, 0.0\}$ (Fig. 4d). Both MUAS and MCAS methods cluster in such regions mainly LF training points, while MFEI and ACAS methods provide also a less significant clusterization of HF training points. Figure 5 shows the velocity contours of the optimal hydrofoil shape identified by the adaptive sampling methods. The differences of the hydrofoil shapes are not evident, although the velocity contours are considerably different.

The results of the adaptive sampling procedure are summarized in Tab.1, showing how MFEI methods results to be the most effective adaptive sampling technique, for the present problem.

5 CONCLUSIONS AND FUTURE WORK

Four adaptive sampling methods for multi-fidelity metamodeling are presented and applied to the CFD-shape optimization of a NACA hydrofoil. The multi-fidelity approximation is obtained as the sum of a low-fidelity-trained metamodel and the metamodel of the difference (error) between high- and low-fidelity evaluations. The metamodel is based on SRBF, which provides the prediction and the associated uncertainty. The prediction uncertainty of both the low-fidelity and the error metamodel is used for the adaptive

Table 1: Summary of the performances of the adaptive sampling methods

	$\|\mathcal{L}\|$	$\|\mathcal{E}\|$	Predicted $C_{d,\min}$	x_1	x_2	HF $C_{d,\min}$
MUAS	136	14	7.1759E-3	0.3084	0.0000	7.2582E-3
MFEI	135	15	7.1545E-3	0.3709	0.0000	7.2371E-3
ACAS	138	12	7.1754E-3	0.3620	0.0001	7.2403E-3
MCAS	137	11	7.2816E-3	0.3291	0.0000	7.2606E-3
Reference				0.3554	0.0003	7.2340E-3

refinement of the low- and high-fidelity training sets. The ratio of the computational cost of high- and low-fidelity evaluations affect the choice of the fidelity to sample.

The refinement of the training set is performed following: (i) the minimization of the maximum uncertainty of the multi-fidelity metamodel prediction (MUAS), (ii) the maximization of the expected improvement (computed with a different reference to better comply with the multi-fidelity methodology, MFEI), (iii) minimization of an aggregated merit factor of prediction uncertainty and predicted objective function (ACAS), and (iv) multi-objective optimization maximizing the prediction uncertainty and minimizing the predicted objective function (MCAS). The multi-fidelity metamodel performance has been assessed in terms of convergence of the maximum uncertainty and convergence of the objective function minimum.

The CFD-shape optimization problem of the NACA hydrofoil is resulted to be a challenging problem for the multi-fidelity metamodel. The existence of numerical noise affects the SRBF interpolation, resulting in large uncertainty of the multi-fidelity prediction in noisy regions of the domain. Therefore, the sampling methods that directly take into account the multi-fidelity prediction uncertainty have been "trapped" in adding training points in such region.

Future work includes comparing the current multi-fidelity results with a metamodel trained only with high-fidelity evaluations for all the sampling methods. Furthermore, the effects of $U^{\star}_{\hat{f}}$ on the MCAS method in presence of numerical noise will be assessed, as well as the use of approximation methods (*e.g.* least square fit) as opposed to interpolation. Finally, the CFD simulation procedures will be optimized to reduce the noise at its source.

ACKNOWLEDGMENTS

Development of the adaptive multi-fidelity methodology has been partially supported by the Office of Naval Research, NICOP grant N62909-15-1-2016 and N62909-18-1-2033, administered by Dr. Woei-Min Lin, Dr. Salahuddin Ahmed, and Dr. Ki-Han Kim; by the Italian Flagship Project RITMARE, founded by the Italian Ministry of Education; and by the EU H2020 Project Holiship "HOLIstic optimisation of SHIP design and operation for life cycle", grant N.689074.

REFERENCES

[1] Viana, F. A., Simpson, T. W., Balabanov, V., and Toropov, V. (2014). *Metamodeling in multidisciplinary design optimization: how far have we really come?*. AIAA Journal, **52**(4), 670–690.

[2] Liu, H., Ong, Y. S., and Cai, J. (2017). *A survey of adaptive sampling for global metamodeling in support of simulation-based complex engineering design*. Structural and Multidisciplinary Optimization **57**(1), 393–416.

[3] Volpi, S., Diez, M., Gaul, N. J., Song, H., Iemma, U., Choi, K. K., Campana E. F., and Stern, F. (2015). *Development and validation of a dynamic metamodel based on stochastic radial basis functions and uncertainty quantification*. Structural and Multidisciplinary Optimization, **51**(2), 347–368.

[4] Zhao, L., Choi, K. K., and Lee, I. (2011). *Metamodeling method using dynamic kriging for design optimization*. AIAA journal, **49**(9), 2034–2046.

[5] Diez, M., Volpi, S., Serani, A., Stern, F., and Campana, E. F. (2015). *Simulation-based design optimization by sequential multi-criterion adaptive sampling and dynamic radial basis functions*. In EUROGEN 2015, International Conference on Evolutionary and Deterministic Methods for Design, Optimization and Control with Applications to Industrial and Societal Problems.

[6] Ng, L. W. T., and Eldred, M. (2012). *Multifidelity uncertainty quantification using non-intrusive polynomial chaos and stochastic collocation*. In 53rd AIAA/ASME/ASCE/AHS/ASC Structures, Structural Dynamics and Materials Conference.

[7] Zheng, J., Shao, X., Gao, L., Jiang, P., and Li, Z. (2013). *A hybrid variable-fidelity global approximation modelling method combining tuned radial basis function base and kriging correction*. Journal of Engineering Design, **24**(8), 604–622.

[8] De Baar, J., Roberts, S., Dwight, R., and Mallol, B. (2015). *Uncertainty quantification for a sailing yacht hull, using multi-fidelity kriging*. Computers & Fluids, **123**, 185–201.

[9] Pellegrini, R., Iemma, U., Leotardi, C., Campana, E. F., and Diez, M. (2016). *Multi-fidelity adaptive global metamodel of expensive computer simulations*. In 2016 IEEE Congress on Evolutionary Computation (CEC), 4444–4451.

[10] Pellegrini, R., Serani, A., Broglia, R., Diez, M., and Harries, S. (2018). *Resistance and Payload Optimization of a Sea Vehicle by Adaptive Multi-Fidelity Metamodeling*. In AIAA/ASCE/AHS/ASC Structures, Structural Dynamics, and Materials Conference, 2018.

[11] Jones, D. R., Schonlau, M., and Welch, W. J. (1998). *Efficient global optimization of expensive black-box functions*. Journal of Global optimization, **13**(4), 455–492.

[12] Serani, A., Leotardi, C., Iemma, U., Campana, E. F., Fasano, G., and Diez, M. (2016). *Parameter selection in synchronous and asynchronous deterministic particle swarm optimization for ship hydrodynamics problems*. Applied Soft Computing, **49**, 313–334.

[13] Pellegrini, R., Serani, A., Leotardi, C., Iemma, U., Campana, E. F., and Diez, M. (2017). *Formulation and parameter selection of multi-objective deterministic particle swarm for simulation-based optimization*. Applied Soft Computing, **58**, 714–731.

[14] Huband, S., Hingston, P., Barone, L., and While, L. (2006). *A review of multiobjective test problems and a scalable test problem toolkit*. IEEE Transactions on Evolutionary Computation, **10**(5), 477–506.

[15] Durand, M. (2012). *Interaction fluide-structure souple et légère, application aux voiliers*. Ph.D. thesis, Ecole Centrale de Nantes.

[16] Wackers, J., Deng, G., Guilmineau, E., Leroyer, A., Queutey, P., Visonneau, M., Palmieri, A. and Liverani, A., (2017). *Can adaptive grid refinement produce grid-independent solutions for incompressible flows?*. Journal of Computational Physics, **344**, 364–380.

[17] George, P. L. and Borouchaki, H., (1998). *Delaunay triangulation and meshing Application to Finite Elements*. Hermes.

[18] Ploé, P., Lanos, R., Visonneau, M., and Wackers, J., (2017). *Bayesian strategies for simulation based optimisation and response surface creation using a single tool*. Application to hydrofoil optimisation. In Proc. of 7th International Conference on Computational Methods in Marine Engineering (MARINE 2017), Nantes, France, 15-17 May.

[19] Wackers, J., Queutey, P., Visonneau, M., Pellegrini, R., Serani, A., and Diez, M. (2018) *CFD-Based Shape Optimization Under Limited Computational Resources a Study on Adaptive Multi-Fidelity Metamodeling*. To appear in proceedings of 17th Conference on Computer Applications and Information Technology in the Maritime Industries (COMPIT 2018), 14-16 May, Pavone, Italy.